Mitigating the Climate Forcing of Aircraft Contrails by Small-Scale Diversions and Technology Adoption

Roger Teoh[1], Ulrich Schumann[2], Arnab Majumdar[1] and Marc E.J. Stettler[1]*

[1] Centre for Transport Studies, Department of Civil and Environmental Engineering, Imperial College London, London, SW7 2AZ, United Kingdom

[2] Deutsches Zentrum für Luft- und Raumfahrt, Institute of Atmospheric Physics, 82234 Oberpfaffenhofen, Germany

* Corresponding author: m.stettler@imperial.ac.uk

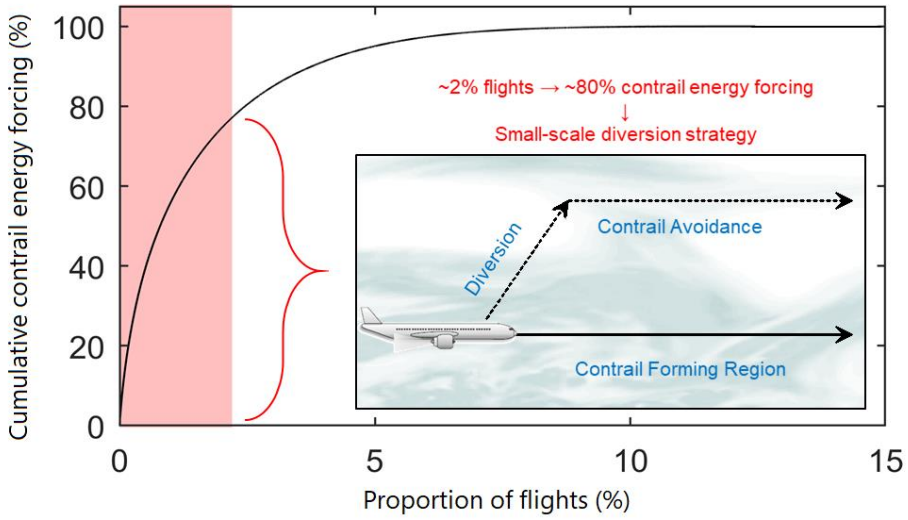

Abstract

The climate forcing of contrails and induced-cirrus cloudiness is thought to be comparable to the cumulative impacts of aviation CO_2 emissions. This paper estimates the impact of aviation contrails on climate forcing for flight track data in Japanese airspace and propagates uncertainties arising from meteorology and aircraft black carbon (BC) particle number emissions. Uncertainties in contrail age, coverage, optical properties, radiative forcing and energy forcing (EF) from

individual flights can be two orders of magnitude larger than the fleet-average values. Only 2.2% [2.0%, 2.5%] of flights contribute to 80% of the contrail EF in this region. A small-scale strategy of selectively diverting 1.7% of the fleet could reduce the contrail EF by up to 59.3% [52.4%, 65.6%], with only a 0.014% [0.010%, 0.017%] increase in total fuel consumption and CO_2 emissions. A low-risk strategy of diverting flights only if there is no fuel penalty, thereby avoiding additional long-lived CO_2 emissions, would reduce contrail EF by 20.0% [17.4%, 23.0%]. In the longer term, widespread use of new engine combustor technology, which reduces BC particle emissions, could achieve a 68.8% [45.2%, 82.1%] reduction in the contrail EF. A combination of both interventions could reduce the contrail EF by 91.8% [88.6%, 95.8%].

Keywords: Contrail cirrus, Aviation, Black Carbon, Meteorology, Climate forcing

1 INTRODUCTION

Contrails are line-shaped clouds that form behind aircraft at favourable atmospheric conditions[1,2]. At cruising altitudes, aircraft black carbon (BC) particle emissions act as the primary source of condensation nuclei for the formation of contrail ice particles[3]. Most contrails have a short atmospheric lifetime and sublimate during or shortly after the decay of the aircraft wake vortex[4]. Under ice super-saturated conditions, however, contrails persist, spread and mix with other contrails and natural cirrus, transitioning into contrail cirrus which could have lifetimes of up to 18 h[5]. Several studies estimate that the global contrail coverage is around 0.1% to 0.4%[6–8], and possibly 10%[9,10] in regions with high air traffic density (ATD).

During the day, contrails can cause a cooling effect by reflecting incoming shortwave (SW) solar radiation back to space, while trapping and re-emitting longwave (LW) infrared radiation back to

the Earth's surface at all times[11]. The most common metric used to quantify the contrail climate forcing is the radiative forcing (RF), which describes the instantaneous change in energy flux caused by contrails at the top of the atmosphere per unit area (globally or in a specified spatial domain) and time[12]. The contrail net RF is strongly dependent on the meteorological conditions, contrail characteristics, surface albedo, natural cirrus properties and coverage, as well as diurnal and seasonal cycles[2,11–14]. Globally, the annual mean net RF of contrail cirrus is estimated to range from 0.01 to 0.09 W m^{-2}, comparable to the integrated historical CO_2 emissions from aviation activity (0.015 to 0.04 W m^{-2})[15], and could exceed 1 W m^{-2} over regions with high ATD[9,14–17]. The large uncertainty in contrail cirrus RF is due to uncertainties in spatial distribution, contrail properties and radiative transfer schemes[18].

An alternative metric that has been used to quantify the contrail climate forcing is the energy forcing (EF, in units of J) or the EF per flight distance (J m^{-1})[12,16,19]. It is defined as the product of the local contrail RF (RF′, the change in energy flux per contrail area)[13,20], length (L) and width (W), integrated over its lifetime (t),

$$\text{Contrail EF [J]} = \int_0^t \text{RF}'(t) \times L(t) \times W(t)\, \mathrm{d}t\ . \qquad (1)$$

The EF measures the contrail climate forcing arising from individual flights. The EF per unit length of contrail was estimated[16] to be between -4 and 24 $\times 10^8$ J m^{-1} with a mean of 0.25 $\times 10^8$ J m^{-1}.

Various models have been developed to estimate the characteristics and climate forcing of contrails, ranging from large eddy simulations (LES)[21–24] to atmospheric general circulation models (GCM)[6,7]. However, LES requires large computational times, while GCMs only provide aggregated contrail outputs at a grid box level. The Contrail Cirrus Prediction Model (CoCiP)[8] and Contrail Evolution and Radiation Model (CERM, a derivative of CoCiP)[25] utilises parameterised

physics to model the contrail segments produced by individual flights. While the BC number emissions index (EI_n) is an essential input parameter for contrail models[8], previous implementations of CoCiP and CERM have assumed a constant EI_n of 10^{15} kg^{-1}. To improve upon this assumption, the Fractal Aggregates (FA) model[26] or the Smoke Correlation for Particle Emissions CAEP11 (SCOPE11)[27] methodology, capable of estimating the EI_n from the BC mass emissions index (EI_m) for specific aircraft-engine types and engine powers, can be incorporated into CoCiP or CERM to more accurately represent aircraft emissions.

Contrail models are vital in validating the effectiveness of different mitigation solutions such as the use of alternative fuels, new engine technology and flight diversion strategies[25,28–33]. However, uncertainties in the estimated contrail properties must be modelled to more accurately quantify the potential net climate benefits from implementing these mitigation solutions.

This paper therefore aims to: (i) improve upon existing contrail models by applying the FA model to CoCiP to improve estimates of the aircraft BC EI_n and contrail properties; (ii) evaluate the uncertainty of the contrail climate forcing due to uncertainties in BC EI_n and meteorology; and (iii) propose solutions to mitigate the contrail climate forcing in the Japanese airspace.

2 MATERIALS & METHODS

Here we describe the methods to evaluate contrail climate forcing and two mitigation proposals. In summary: (i) the aircraft activity dataset is provided by the CARATS Open Data for Japan; (ii) aircraft fuel consumption is estimated using the Base of Aircraft Data 3 (BADA3); (iii) the FA model is used to estimate the aircraft BC EI_n; (iv) uncertainties in contrail characteristics and climate forcing are modelled by implementing CoCiP with a Monte Carlo simulation; and (v) meteorological data is from the European Centre for Medium-Range Weather Forecast (ECMWF)

ERA5 high resolution realisation (HRES) reanalysis and the ERA5 ten-member ensemble (EDA). Details and data omitted from the main text are included in the Supporting Information (SI).

2.1 Proposals for Contrail Mitigation

We simulate contrails that were produced by individual flights over Japan and evaluate two proposals to reduce the contrail climate forcing: (i) a small-scale strategy of diverting flights with the largest contrail EF; and (ii) widespread adoption of aircraft powered by cleaner engine technologies such as the double annular combustor (DAC).

For proposal (i), we do not attempt to avoid all contrails, instead we reduce the potential warming impacts corresponding to positive contrail EF by implementing a targeted diversion strategy. First, we quantify the proportion of flights that contribute to 80% of the total contrail EF. For these flights, we generate alternative trajectories (± 2000 feet in cruising altitude) and pick the trajectory with the lowest EF (which could be negative). We then aggregate the EF from all flights to quantify the percentage reduction in contrail EF for the fleet and the difference in total fuel consumption (TFC) between the original and diverted trajectories.

For proposal (ii), we simulate a hypothetical scenario where all aircraft are assumed to be powered by DACs, which have been shown to have significantly lower BC EI_n compared to conventional singular annular combustors (SAC): ground measurements show that the EI_n emitted by DACs at low engine powers (pilot stage) is comparable to SACs, but decreases by an order of magnitude (to $10^{13} – 10^{14}$ kg^{-1}) at higher engine powers (lean combustion mode)[34,35]. To be conservative, the engine efficiency and fuel consumption for DACs are assumed to be the same as for SACs.

Further methodological details for these proposals are in the SI §S6 and §S7.

2.2 Aircraft Activity Dataset

The CARATS Open Data is a high-resolution aircraft activity dataset providing flight track data from the Japanese airspace. Six one-week periods of air traffic data are recorded bimonthly from May-2012 to Mar-2013, including 61 million waypoints. For each flight, a censored flight ID and an International Civil Aviation Organisation (ICAO) aircraft type designator are provided, and their 3D position is tracked approximately every 10 s. As contrail properties are spatially dependent on aircraft trajectory, a high-resolution dataset is advantageous relative to other studies: (i) the AERO2K dataset provides monthly aggregated data and does not provide disaggregated trajectories from individual flights[36]; (ii) radar track data from the Aviation Environmental Design Tool (AEDT)[37] has an inconsistent temporal resolution; while (iii) the Aviation Emissions Inventory Code (AEIC) assumes a great circle flight path between airport pairs[38].

However, limitations of the CARATS Open Data include waypoints with erroneous spatial data and incomplete trajectories for international flights when their positions are outside the Japanese airspace[39]. To overcome this, we applied a series of data cleaning and correction steps to estimate the rate of climb and descent, true airspeed and Mach number for each waypoint, which are detailed in the SI §S2.

2.3 Aircraft Fuel Consumption & Thrust Settings

BADA3 (ref.[40]) is used to estimate the fuel mass flow rate ($\dot{m}_f$) for each waypoint, and the TFC of each flight. Aircraft-engine assignments are taken from an earlier study[41], and the initial aircraft mass is estimated assuming an average aircraft load factor of 75%[42]. Further description of BADA3 is in SI §S2.3.

The $\dot{m}_f$ for one flight, validated against an independent study[39] (SI §S2.3), are in good agreement: the estimated $\dot{m}_f$ of individual waypoints at cruise agree to ± 10%, and the estimated TFC is within

± 3%. However, we note two limitations of BADA3: (i) a decrease in the accuracy of the modelled $\dot{m}_{\mathrm{f}}$ at suboptimal flight conditions (suboptimal altitudes and high speeds)[43]; and (ii) a comparison with the actual $\dot{m}_{\mathrm{f}}$ from flight data recorders showed that the uncertainty in $\dot{m}_{\mathrm{f}}$ (from BADA3) is larger at climb and descent[44]. For this study, limitation (ii) is of minor importance because contrails predominantly form at cruise. However, limitation (i) remains an open issue and BADA4, which was developed as an improvement to BADA3, was not accessible.

Following the estimation of $\dot{m}_{\mathrm{f}}$, the engine thrust settings ($\frac{F}{F_{00,\mathrm{max}}}$, where $F_{00,\mathrm{max}}$ is the maximum rated thrust at sea level and zero speed) are estimated assuming[45–48] that $\frac{F}{F_{00,\mathrm{max}}}$ is approximately equal to the ratio of $\dot{m}_{\mathrm{f}}$ to the fuel flow at $F_{00,\mathrm{max}}$ ($\frac{\dot{m}_{\mathrm{f}}}{\dot{m}_{\mathrm{f,max}}}$, where $\dot{m}_{\mathrm{f,max}}$ is obtained from the ICAO Aircraft Emissions Databank[49]). We note that the $\frac{F}{F_{00,\mathrm{max}}}$ (or $\frac{\dot{m}_{\mathrm{f}}}{\dot{m}_{\mathrm{f,max}}}$) is used to estimate BC $\mathrm{EI_n}$ and so uncertainty in this assumption may propagate. Further discussion is in the SI §S2.3 and §S3.2.

2.4 Estimating the BC Number Emissions Index from Aircraft

The FA model[26] is used to estimate the aircraft BC $\mathrm{EI_n}$,

$$\mathrm{EI_n} = \frac{\mathrm{EI_m}}{\rho_0 (\frac{\pi}{6}) (k_{\mathrm{TEM}})^{3-D_{\mathrm{fm}}} \mathrm{GMD}^{\varphi} \exp\left(\frac{\varphi^2 \ln(\mathrm{GSD})^2}{2}\right)}, \quad (2)$$

$$\text{where } \varphi = 3D_{\mathrm{TEM}} + (1 - D_{\mathrm{TEM}}) D_{\mathrm{fm}},$$

where $\mathrm{EI_m}$ is the BC mass emissions index, ρ_0 is the BC material density, D_{fm} is the mass-mobility exponent of BC aggregates, GMD and GSD are the geometric mean diameter and standard deviation of a given BC particle size distribution, while k_{TEM} and D_{TEM} are prefactor-exponent coefficients. The FA model is compared to the SCOPE11[27] and is selected due to better

performance when validated against ground and cruise measurements of BC emissions[32,34]. Further methodological details are included in SI §S3.

Given that the inputs required by the FA Model (i.e. EI_m, GMD and GSD) are only measured for a small number of aircraft-engine combinations predominantly on the ground, existing models and datasets are reviewed to select or develop relationships to predict these parameters at cruise (SI §S3.2). In summary: (i) the Formation and Oxidation (FOX)[47] and the Improved FOX (ImFOX)[45] methods are used to estimate lower and upper bounds of EI_m for conventional SACs, respectively, and following comparison between measurements and estimates of EI_m at cruise, we enlarge the uncertainty bound by -20% of the FOX and +50% of the ImFOX estimates to reflect significant uncertainties; (ii) the ratio of turbine inlet to compressor inlet temperatures (T_4/T_2) is used to estimate EI_m for DACs in the pilot stage ($T_4/T_2 < 2.85$) and constant value (3.25 mg kg^{-1}) for the lean combustion stage ($T_4/T_2 \geq 2.85$); (iii) the GMD for both engine types are also estimated as a function of T_4/T_2 and comparisons are made to measurements to estimate a 95% confidence interval (CI) of ±20%; (iv) constant GSD (1.80), D_{fm} (2.76), k_{TEM} (1.621×10^{-5}) and D_{TEM} (0.39) are assumed at cruise; and (v) particle sampling losses are corrected for and EI_n at the engine exit plane is estimated by substracting a correction factor δ_{loss} from the GMD, assumed to be uniformly distributed between 3 and 8.5 nm, which implicitly assumes that sampling losses predominantly affect the smallest particles causing an increase in the GMD at the instrument measurement point and that the reduction to EI_m is negligible. For the baseline scenario, the list to identify DAC aircraft is in the SI §S2.4.

2.5 Contrail Model and Meteorology

CoCiP is used to simulate the characteristics and climate forcing of contrails produced by individual flights. Further details on CoCiP are given in the literature[8,20] and in the SI §S4.

Two improvements to CoCiP were implemented in this study. Firstly, the FA model enables the EI_n to be estimated for each waypoint as a function of aircraft type and $\frac{F}{F_{00,\max}}$, which is an improvement relative to previous studies which assumed a constant EI_n for every waypoint; Secondly, two distinct meteorological datasets are used: the ERA5 HRES contains nominal meteorological data at a very high spatial (0.25° × 0.25°) and temporal resolution (hourly); while the ERA5 EDA provides 10-member ensemble means and standard deviations to account for observational, model and boundary condition uncertainties in the reanalysis but at a lower spatial (0.5° × 0.5°) and temporal resolution (3-hourly). The ERA5 EDA is validated with meteorological data from the Measurement of Ozone and Water Vapour by Airbus in-service aircraft (MOZAIC) campaign (SI §S4.3): both datasets are generally in good agreement where the R^2 is between 0.434 and 0.995.

2.6 Uncertainty Propagation

We implemented CoCiP with a Monte Carlo simulation to quantify uncertainties of the simulated contrail characteristics and climate forcing arising from uncertainties in aircraft BC EI_n and meteorology. As detailed in the SI§S3.4 and §S4.4, uncertainties in the FA model inputs are treated as independent, leading to a [-70%, +200%] uncertainty in estimated EI_n (95% CI) that is lognormally distributed, while meteorological uncertainties from the ERA5 EDA are normally distributed[50]. The ranges of contrail properties (with uncertainty bounds) are compared with the results from a nominal run of CoCiP using the ERA5 HRES, which has a higher spatiotemporal resolution. We also note that the TFC uncertainty includes uncertainties in the ambient temperature (T_{amb}) and wind speed.

The number of Monte Carlo simulations is restricted by computational demands: one CoCiP run for the full set of aircraft trajectories takes 5 h. To increase the rate of convergence, we use a quasi-

random low-discrepancy Sobol sequence scrambled using the Matousek-Affine-Owen algorithm. Results show that the CoCiP contrail outputs converge to within 1% after 100 runs (SI §S4.4).

The uncertainties explored in this paper are limited to meteorology and the aircraft BC EI_n. We note that further uncertainties exist between different contrail models, but a multi-model comparison is out of scope of this paper.

2.7 Comparing Climate Forcing of CO_2 and Contrails

The diversion of flights raises a trade-off between minimising the contrail climate forcing and increase in TFC (and CO_2 emissions). We note that the comparability of the long-term climate impacts of contrails and CO_2, in terms of the global surface temperature response, remains an open issue because of: (i) large uncertainties in the contrail efficacy[51–54] (quantifying it is beyond our research scope); (ii) differences in time horizons (TH); and (iii) a lack of consensus on a common metric. While these limitations are acknowledged, we used the absolute global warming potential (AGWP) for pulse emissions to derive the CO_2 EF emitted from individual flights for comparison with the contrail EF,

$$\mathrm{CO_2\ EF\ [J]} = \int_0^{\mathrm{TH}} \mathrm{RF_{CO_2}} \mathrm{d}t \times \mathrm{S_{Earth}} = [\mathrm{AGWP_{100}} \times (365 \times 24 \times 60^2)] \times \mathrm{TFC} \times \mathrm{EI_{CO_2}} \times \mathrm{S_{Earth}}, \quad (3)$$

where $\mathrm{EI_{CO_2}}$ is the emissions index for CO_2 (3.16 kg kg^{-1})[37], $\mathrm{S_{Earth}}$ (5.101×10^{14} m^2)[55] is the surface area of Earth as CO_2 gets well-mixed over Earth's atmosphere, and an AGWP with a 100-year TH ($AGWP_{100}$ = 92.5 [68, 117] $\times 10^{-15}$ yr Wm^{-2} per kg-CO_2)[56] is used to align with the Kyoto Protocol. The AGWP integrates the CO_2 RF over a determined TH, accounting for the decay in CO_2 RF over time[56]. From Eq. (3), the CO_2 EF per mass of fuel burned can be estimated as 4.70 [3.45, 5.95] $\times 10^9$ J kg^{-1}. For a mean fuel consumption of 7.26 kg km^{-1} (estimated in this study), the CO_2 EF per flight distance is 3.41 [2.50, 4.32] $\times 10^7$ J m^{-1}. This value serves as a reference to

compare with the contrail EF per flight distance. Sensitivity of the CO_2 EF to TH will be evaluated by using a 20- and 100-year AGWP TH[56].

The contrail EF is approximated with Eq. (1), and the choice of TH does not influence the contrail EF because of their short lifetimes (< 24 h).

3 RESULTS

3.1 Aircraft Black Carbon Particle Number Emissions

Over the six one-week periods, the average EI_n for: (i) the entire dataset is 1.37 [1.35, 1.39] $\times 10^{15}$ kg^{-1}; (ii) aircraft equipped with SACs (84% of flights in the dataset) is 1.59 [1.57, 1.62] $\times 10^{15}$ kg^{-1}; and (iii) aircraft powered by DACs (16% of flights) is 0.38 [0.37, 0.39] $\times 10^{15}$ kg^{-1} with a 95% CI. Measurements of EI_n at cruise range from 0.2 to 0.8 $\times 10^{15}$ kg^{-1}, however these were not corrected for particle sampling losses[32,57,58]. Our estimate of fleet-average EI_n is higher as we account for sampling losses using a δ_{loss} factor (described in Section 2.4 and SI §S3.2). The estimated fleet-average EI_n would reduce to 0.65 $\times 10^{15}$ kg^{-1} if we do not account for sampling losses ($\delta_{loss} = 0$), which is within the range of measurement data. However, as previous contrail studies have inferred the EI_n to be $>10^{15}$ kg^{-1} in order to achieve best agreement between modelled and in-situ measured and satellite-observed contrail properties[8,17,59–62], we proceed with our estimate including sampling losses.

For individual aircraft, changes in the estimated EI_n across different phases of flight are presented in SI §S3.5: uncertainties in the estimated EI_n for each waypoint, [-70%, +200%], are significantly larger than the EI_n uncertainties for the entire fleet [-1.65%, +1.24%] because of the law of large numbers, where uncertainties from different flights cancel out when aggregated into a fleet-averaged EI_n.

3.2 Contrail Characteristics and Climate Forcing

Hourly outputs for six selected contrail parameters are presented in Figure 1, while the fleet-average values are summarised in Table 1. On average, when contrails are simulated using the ERA5 EDA: (i) 17.8% [17.2%, 18.4%] of flights form contrails; (ii) the percentage of flight distance with contrails is 7.15% [6.65%, 7.42%]; (iii) the mean contrail segment age for a given Monte Carlo simulation is 3.24 [3.09, 3.36] h; (iv) the optical depth (τ) is 0.143 [0.139, 0.151]; (v) the net contrail RF and EF are 1.74 [1.21, 2.56] W m^{-2} and 5.38 [3.85, 6.66] $\times 10^{18}$ J respectively; and (vi) only 2.19% [1.97%, 2.45%] of flights are responsible for 80% of the contrail EF. The contrail EF per flight distance (5.35 [3.82, 6.62] $\times 10^{7}$ J m^{-1}) is 1.6 times higher than the CO_2 EF (3.41 [2.50, 4.32] $\times 10^{7}$ J m^{-1}, 100-year TH) despite the short contrail lifetimes relative to CO_2. Histograms show that the uncertainties of contrail properties are either normal or lognormally distributed (SI §S5).

When contrails are simulated using the ERA5 HRES, Table 1 shows that 10 out of the 14 outputs are within the uncertainty bounds of the EDA. However, the total number and percentage of flights forming contrails are 13% higher, the mean contrail segment age is 7% smaller, and τ is 8% larger relative to the EDA results. This is likely due to the higher spatiotemporal resolution of the HRES capturing localised pockets of ice supersaturated regions (ISSRs) which causes a higher number of flights forming shorter-lived contrail segments with a larger τ (Table 1). The hourly outputs using the HRES are within the uncertainty bounds of the EDA (Figure 1). Furthermore, the simulated contrail properties are generally comparable with the range of observed and modelled values reported in the literature[16,17,60,63].

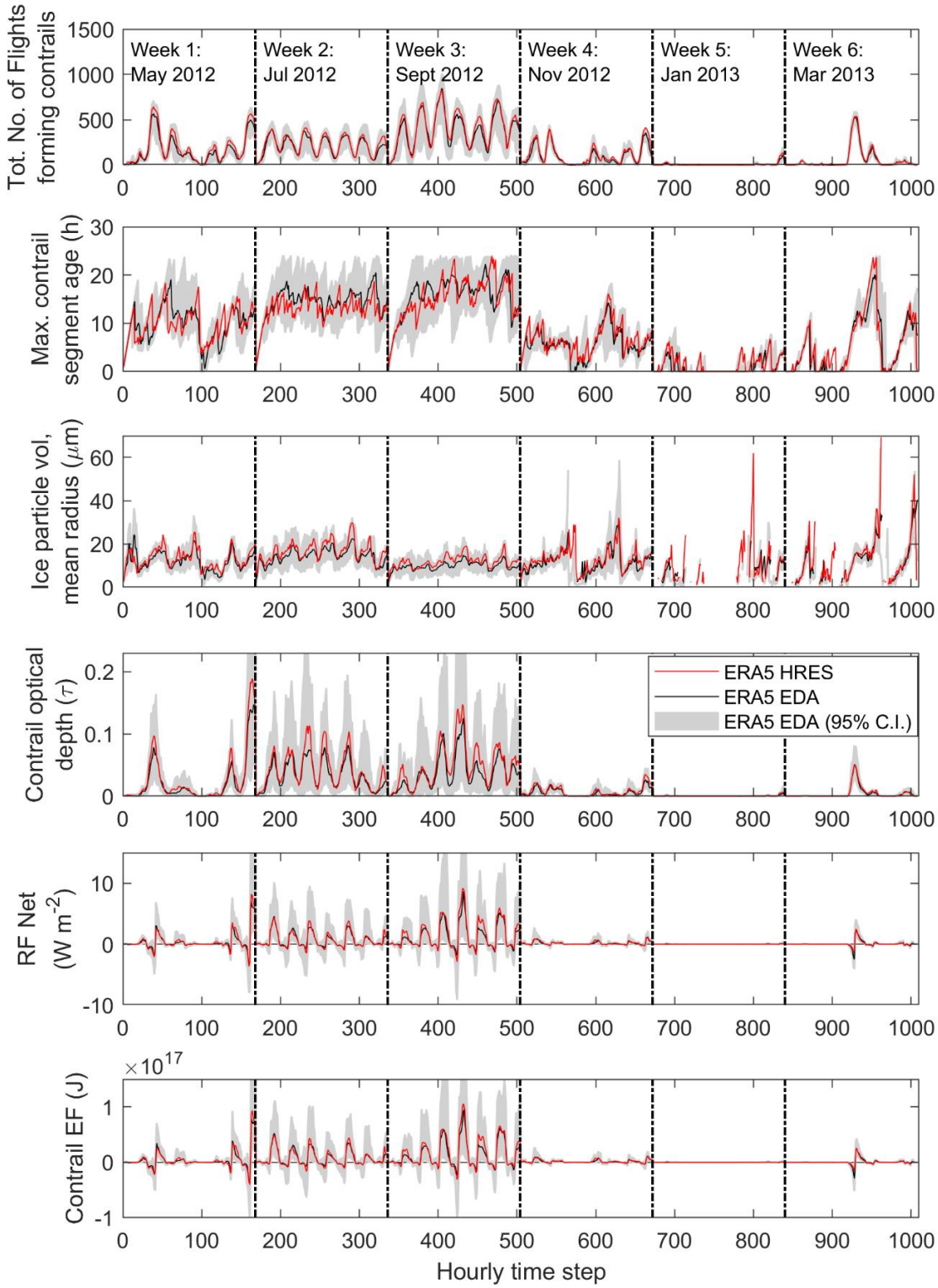

Figure 1: The characteristics and climate forcing of contrails in the Japanese airspace over time (hourly time step, covering 6 weeks of simulations distributed over a year). Contrails are simulated with CoCiP using meteorological inputs from the ERA5 HRES (red line) and the EDA (black lines, and the shaded region represents the 95% CI for the particular time step). For other parameters that are not presented in this figure, the reader is referred to the SI §S5.

Table 1: Fleet-average contrail characteristics and climate forcing over the six weeks of data available, which are simulated with CoCiP using meteorological inputs of the ERA5 EDA (100 Monte Carlo simulations, 95% CI provided) and the HRES (Nominal).

CoCiP Outputs (6 weeks, Fleet average)	ERA5 EDA (n=100)				ERA5 HRES
	Mean	$P_{2.5\%}$	$P_{97.5\%}$	95% CI w.r.t. Mean	Nominal
Total number of flights forming contrails	26534	25662	27385	[-3.29%, +3.21%]	29875
% of flights forming contrails	17.8	17.2	18.4	[-3.26%, +3.20%]	20.0
% of flight distance forming contrails	7.15	6.65	7.42	[-6.88%, +3.89%]	7.37
Mean contrail segment age (h)	3.24	3.09	3.36	[-4.57%, +3.80%]	3.01
Maximum contrail segment age (h)	23.9	23.6	24.0	[-1.54%, +0.13%]	23.9
Ice particle volume mean radius (μm)	13.3	12.7	13.8	[-4.51%, +3.68%]	13.0
Contrail optical depth (τ)	0.143	0.139	0.151	[-2.87%, +5.45%]	0.154
SW RF (W m^{-2})	-4.42	-4.65	-3.99	[-5.27%, +9.82%]	-4.48
LW RF (W m^{-2})	6.16	5.87	6.54	[-4.73%, +6.22%]	6.39
Net RF (W m^{-2})	1.74	1.21	2.56	[-30.2%, +46.8%]	1.91
Contrail EF (× 10^{18} J)	5.38	3.85	6.66	[-28.5%, +23.7%]	5.31
EF per flight distance (× 10^{8} J m^{-1})	0.535	0.382	0.662	[-28.6%, +23.7%]	0.421
EF per contrail length (× 10^{8} J m^{-1})	7.50	5.33	9.53	[-29.0%, +27.1%]	7.17
% flights responsible for 80% contrail EF	2.19	1.97	2.45	[-9.95%, 12.0%]	2.44

Table 2: Range of contrail characteristics and climate forcing produced by a Boeing B747-400 on the 11th of July 2012 (FLT2429), which are simulated with CoCiP using meteorological inputs of the ERA5 EDA (100 Monte Carlo simulations, 95% CI provided) and the HRES (Nominal). Data on the flight trajectory and histograms showing the uncertainty distribution of each parameter is in the SI §S5.

CoCiP Outputs (Single Flight)	ERA5 EDA (n=100)				ERA5 HRES
	Mean	$P_{2.5\%}$	$P_{97.5\%}$	95% CI w.r.t. Mean	Nominal
% of flights segments forming contrails	85.8	15.6	88.4	[-81.9%, +2.97%]	69.1
Mean contrail segment age (h)	8.10	1.01	10.6	[-87.5%, +30.7%]	8.14
Maximum contrail segment age (h)	12.8	3.19	16.2	[-75.1%, +26.4%]	12.4
Ice particle volume mean radius (μm)	11.4	2.67	19.6	[-76.6%, +71.8%]	16.8
Contrail optical depth (τ)	0.104	0.044	0.202	[-57.4%, +95.4%]	0.186
SW RF′ (W m^{-2})	-2.32	-7.99	-0.130	[-244%, +94.4%]	-2.64
LW RF′ (W m^{-2})	4.77	1.03	9.77	[-78.5%, +105%]	9.67
Net RF′ (W m^{-2})	2.60	-1.51	7.14	[-158%, +175%]	5.69
Contrail EF (× 10^{15} J)	4.33	-0.010	17.1	[-100%, +296%]	13.3
EF per flight distance (× 10^{9} J m^{-1})	3.52	-0.008	13.5	[-100%, +296%]	9.29
EF per contrail length (× 10^{9} J m^{-1})	4.59	-0.017	16.2	[-100%, +254%]	13.5

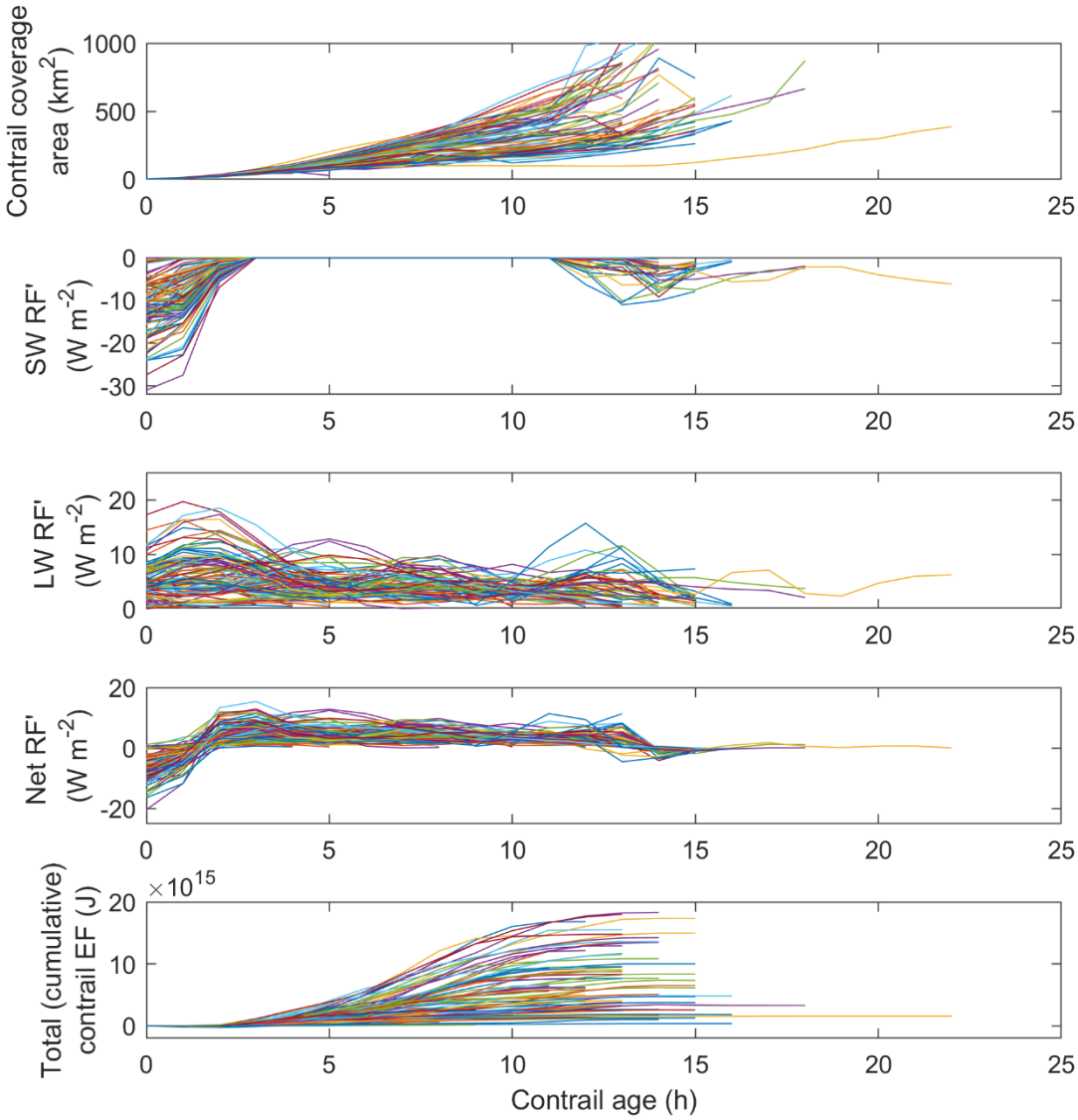

Figure 2: Temporal evolution of the characteristics and climate forcing of contrails produced by a Boeing B747-400 (FLT2429, 11th July 2012). The individual lines represent the results from each Monte Carlo simulation (100 runs in total) using the ERA5 EDA meteorological dataset. The initial contrail segments for this flight (contrail age = 0 h) are formed at 16:30 Japan local time.

Table 2 shows the range of contrail parameters that was produced by a single flight, where the nominal values of all parameters simulated with HRES inputs are within the uncertainty bounds provided by the EDA. This particular flight is selected because the nominal contrail EF is the highest in the dataset. CoCiP estimates a 96% probability of this flight forming contrails, and when contrails are formed, the probability of producing a negative contrail EF (cooling) is 6.25%. Figure 2 shows the temporal evolution of various contrail properties: given that the contrails from this

277 flight were initially formed at 16:30 local time, a negative net RF′ is observed up until dusk (around
278 19:00). However, due to the small contrail coverage area (≈ 10 km^2), this negative net RF′ causes
279 a negligible cooling effect (EF ≈ -0.43 [-2.53, 0.70] $\times 10^{14}$ J) in the first two hours. During the night,
280 the EF starts to increase because of the increasing contrail coverage area and positive net RF′,
281 which stays positive until dawn (around 05:00). We note that the uncertainty bounds of different
282 contrail properties arising from individual flights can be up to two orders of magnitude larger than
283 the fleet-average because the uncertainties cancel out when aggregated across the fleet.

284 **3.3 Mitigation Proposals**

285 The fleet-aggregated contrail, CO_2, and total EF for all scenarios are presented in Table 3.

286 **Small-scale Diversion Strategy**

287 Several studies have evaluated different flight diversion strategies to minimise the formation of
288 contrails by avoiding ISSRs[28–31]. However, a fleet-wide diversion strategy is neither practical nor
289 necessary given that only 2.2% of flights contribute to 80% of the total contrail EF (Table 1).

290 In the short term, a small-scale strategy which selectively diverts flights with the largest EF could
291 significantly reduce the contrail climate forcing, minimise disruptions to air traffic management
292 (ATM) and be implemented quickly without technological changes. Figure 3 shows the flights (for
293 the week in July-2012) that contribute to 80% of the total contrail EF. The average ATD above
294 20,000 feet is used to approximate the free airspace capacity that could be available for a diversion.
295 Figures 3 and S33 (SI §S6.1) show that flights with the largest contrail EF predominantly form
296 between 15:00 and 06:00 local time because contrails formed late in the afternoon would have
297 spread to a large coverage area by nightfall with a positive net RF (similar to Figure 2). The EF
298 typically increases with contrail age, and contrails with the largest EF typically survive longer than
299 10 h.

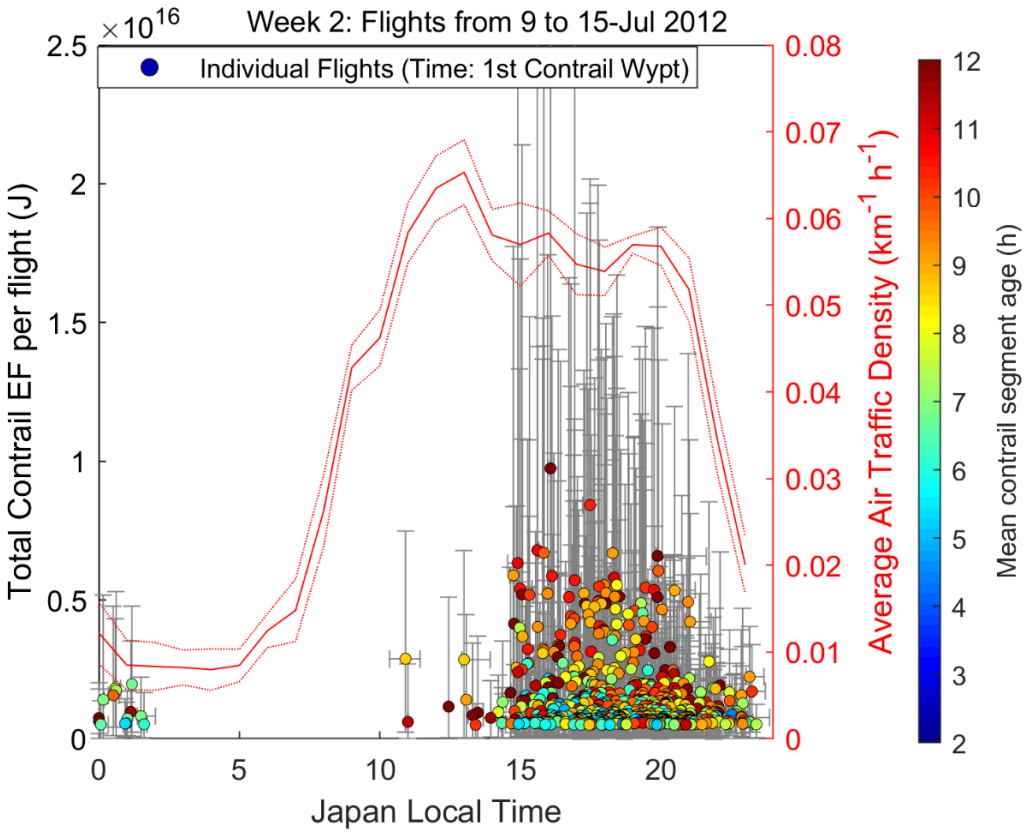

Figure 3: Flights in Week 2 (July 2012) that contribute to 80% of the total contrail EF and the times of day when these flights occur. Error bars denote the 95% CI. For each flight, the mean contrail segment age is shown by the symbol colour. The ATD above 20,000 feet (average and standard deviation) at different times of the day is presented on the right axis. All flights in this figure have a positive EF because flights with cooling contrails (EF < 0 J) are excluded. Similar plots for other weeks are presented in the SI §S6.1.

We therefore propose a strategy where diversions are prioritised for flights that contribute to 80% of the total contrail EF, while also accounting for potential constraints in ATM: (i) at times of low ATD (20:00 to 06:00), all of the selected flights are diverted; while (ii) a limited number of flights, ranging from maximum of 1 to 10% of all flights in each time step, are allowed to divert when the ATD is high but not at its peak (< 0.06 km^{-1} h^{-1}, between 15:00 to 20:00). Previous studies found that ISSR's typically have large horizontal (150 ± 250 km) but shallow vertical extensions (of order 1600 feet)[30,64], consistent with our results (Figure S34, SI §S6.1). Therefore, a small change in cruising altitude (±2000 feet) could minimise the flight distance within regions of high humidity, thereby reducing the contrail lifetime and EF.

Table 3: Fleet-aggregated contrail, CO_2 and total EF for the baseline and three mitigation scenarios. The CO_2 and total EF values are dependent on the CO_2 AGWP TH (20, 100 or 1000 years). For the three mitigation scenarios, the percentage change in contrail, CO_2 and total EF are relative to the baseline scenario (Δ).

	Contrail EF (10^{18} J)	CO_2 AGWP TH (years)	CO_2 EF* (10^{18} J)	Total EF (10^{18} J) [contrails + CO_2]
Baseline Scenario	5.38 [3.85, 6.66]	20	0.93326 [0.62062, 1.2309]	6.31 [4.88, 7.57]
		100	3.4277 [1.7187, 5.0480]	8.76 [6.92, 10.8]
		1000	20.185 [8.6413, 31.424]	25.8 [14.2, 36.7]
Diversion	2.15 [1.38, 2.96] Δ = -59.4% [-65.6, -52.4] %	20	0.93338 [0.62071, 1.2310] Δ = +0.014% [+0.010, +0.017] %	3.11 [2.33, 3.93] Δ = -50.1% [-55.4, -44.6] %
		100	3.4282 [1.7259, 5.0488] Δ = +0.014% [+0.010, +0.017] %	5.94 [3.85, 7.22] Δ = -35.6% [-44.2, -27.6] %
		1000	20.188 [8.6425, 31.428] Δ = +0.014% [+0.010, +0.017] %	22.7 [10.7, 33.6] Δ = -12.2% [-23.1, -7.55] %
Fleetwide DAC Adoption	1.68 [1.19, 2.08] Δ = -68.8% [-82.1, -45.2] %	20	0.93326 [0.62062, 1.2309] Δ = 0	2.62 [2.10, 3.09] Δ = -58.4% [-62.4, -54.4] %
		100	3.4277 [1.7256, 5.0480] Δ = 0	5.06 [3.49, 6.67] Δ = -42.2% [-52.9, -32.6] %
		1000	20.185 [8.6413, 31.424] Δ = 0	22.0 [10.4, 33.0] Δ = -14.5% [-26.9, -8.65] %
Diversion + DAC	0.443 [0.152, 0.684] Δ = -91.8% [-95.8, -88.6] %	20	0.93351 [0.62080, 1.2312] Δ = +0.027% [+0.021, +0.033] %	1.38 [1.05, 1.67] Δ = -77.8% [-82.9, -73.0] %
		100	3.4287 [1.7192, 5.0562] Δ = +0.027% [+0.021, +0.033] %	3.89 [2.15, 5.48] Δ = -56.5% [-70.3, -43.9] %
		1000	20.191 [8.6438, 31.433] Δ = +0.027% [+0.021, +0.033] %	20.8 [9.08, 31.9] Δ = -19.5% [-35.9, -11.6] %

* shown to 5 significant figures to allow identification of differences in values

For the six weeks of data, Figure 4a shows that the fleet-aggregated contrail EF is reduced by up to 59.3% [52.4%, 65.6%] by diverting only 1.7% of the flights. On average, contrail EF is reduced by 21.2% by diverting selected flights at night. The remaining 20.8% to 38.1% depend on the

maximum percentage of flights that are allowed to divert during the day (1 to 10% of all flights in each time step), subject to ATM constraints. Due to seasonal variations of the tropopause height, contrail EF is more efficiently reduced when the aircraft is diverted to a lower cruising altitude during the summer months, and vice versa in winter (SI §S6.3). For the weeks in Jan- and Mar-2013, contrails formed only sporadically (Figure 1). Therefore, large reductions in contrail EF are achieved by diverting a very small number of flights: in week 6 (Mar-2013), diverting only 0.5% of the flights that produce warming contrails could reduce the contrail EF by up to 93.1% [70.0%, 134%] with a 33% probability of a net cooling effect (negative EF). Conversely, there was a prolonged contrail outbreak throughout week 3 (Sept-2012) with 37% of all flights forming contrails. Hence, 4.1% of the flights have to be diverted to reduce the contrail EF by 52.4% [43.1%, 63.2%] in this week.

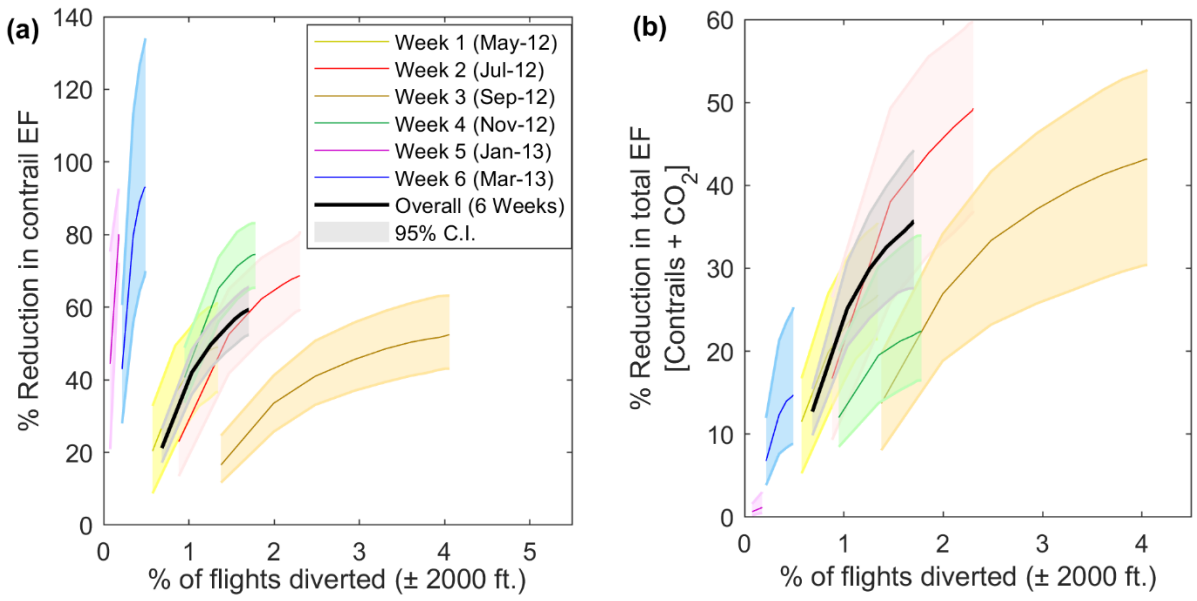

Figure 4: Percentage reduction in the (a) contrail EF and (b) total EF (contrails plus CO_2 EF) vs. the percentage of flights that are diverted by ± 2000 feet. The results are shown for the overall dataset (6 weeks) and separately for specific weeks. The percentage of flights diverted does not fall to 0% because all flights that contribute to 80% of the warming EF are allowed to divert at night.

On average, there is a 0.27% [-0.13%, 0.72%] increase in TFC and CO_2 emissions for each diverted flight (SI §S6.2). The difference in fuel consumption using BADA3 is consistent with the literature, and reflects that modern aircraft are designed with vertical altitude flexibilities of up to 3000 feet at the expense of a few percent fuel penalty[65]. Therefore, diverting 1.7% of flights with a fuel penalty of 0.27% [-0.13%, 0.72%] only translates to a 0.014% [0.010%, 0.017%] increase in fuel consumption (and CO_2 emissions) for the fleet.

If an additional constraint is implemented in each Monte Carlo simulation, such that only the flights that do not incur a fuel penalty are diverted, the maximum reduction in contrail EF that is achievable reduces to 20.0% [17.4%, 23.0%]. This constraint limits the diversion to flights where the original cruise altitude was sub-optimal or those where the alternative trajectory leads to favourable wind conditions.

We assess the mitigation potential for the total EF (contrails plus CO_2): in the baseline scenario 60.8% of the total EF is from contrails (5.38×10^{18} J), while the remaining 39.2% is from CO_2 emissions (3.43×10^{18} J, 100-year TH). Hence, when diverting up to 1.7% of the flights, Figure 4b shows that overall reduction in total EF (35.6% [27.6%, 44.2%]) is less than the reduction in contrail EF (59.3% [52.4%, 65.6%]). For week 5 (Jan-2013), the reduction in total EF is insignificant (1.17% [0.52%, 3.00%]) because contrails form sporadically, and the total EF is dominated by CO_2 emissions from the fleet (SI §S6.3). Table 3 summarises the sensitivity of CO_2 EF and total EF to the AGWP TH: the total EF is reduced by up to 50.1% [44.6%, 55.4%] if a 20-year TH is used; while overall reduction in the total EF is significantly smaller at 12.2% [7.55%, 23.1%] with a 1000-year TH, indicating that a longer TH gives greater weight to CO_2.

Widespread Adoption of Cleaner Engine Technology

Over the longer term, widespread adoption of cleaner-burning DAC engines could also reduce the contrail climate forcing. For the baseline scenario, we separately analysed the distribution of contrail properties produced by SACs and DACs (SI §S7): contrail segments produced by DACs have fewer ice particles with a larger mean radius because the average EI_n from DACs is 76% lower than SACs. This leads to a smaller average age (< 10 h, due to the larger sedimentation rate), τ (< 0.4, due to the Twomey effect) and net RF′ (± 15 W m^{-2}, as the contrail RF′ is proportional to τ) relative to SACs (< 13.5 h, < 0.8 and ± 20 W m^{-2})[12,33,66]. Given the smaller contrail RF′ and lifetime, the mean EF per contrail length (0.55 ×10^8 J m^{-1}) from DACs is 61% smaller when compared to contrails produced by SACs (1.42 ×10^8 J m^{-1}).

When all aircraft are assumed to be DACs (73% reduction in the fleet-average EI_n), the number of contrail-forming flights remains unchanged. However, smaller values are computed for the fleet-average contrail age (-19.5% [-25.3%, -12.5%]), τ (-33.1% [-38.8%, -27.2%]), net RF (-27.4% [-37.7%, -18.9%]) and contrail EF (-68.8% [-82.1%, -45.2%]) relative to the baseline scenario (SI §S7). The reduction in net RF is comparable to previous studies that investigated the effect of changing EI_n: for a 50% reduction in EI_n, Bock & Burkhardt[67] found a 14% reduction in net RF in the Eastern China-Japan region; and for an 80% reduction in EI_n, Burkhardt et al.[33] calculated a 50% reduction in net RF globally. Other studies have investigated the effects of alternative fuels, which also lower EI_n. Generally, reductions in contrail net RF from lower EI_n due to alternative fuels are somewhat offset by increases in water vapour emissions, which facilitate contrail formation[25,67]. If DACs are combined with the diversion strategy, contrail and total EF could be reduced by up to 91.8% [88.6%, 95.8%] and 56.5% [43.9%, 70.3%], respectively, assuming a 100-year TH.

4 IMPLICATIONS

The proposed small-scale diversion strategy could significantly reduce contrail EF with minimal disruption to ATM and increase in CO_2 emissions. This demonstrates the potential to reduce aviation's climate forcing immediately. Although this study is restricted to the Japanese airspace, the qualitative findings are likely valid for other mid-latitude regions.

Significant research gaps remain, and future work should investigate an operational trial, contrail model comparisons, the contrail efficacy and climate impact[51–54,68] (in terms of the global surface temperature response), and further measurements of EI_n at cruise including a range of combustor types and fuels.

Supporting Information

The Supporting Information is available free of charge on the ACS Publications website.

Acknowledgements

The CARATS Open Data was supplied by the Electronic Navigation Research Institute (ENRI). R. Teoh received funding from The Lloyds Register Foundation, and the Skempton Scholarship from the Department of Civil and Environmental Engineering, Imperial College London.

Competing interests' statement

The authors declare no competing interests.

References

1. Kärcher B. Formation and radiative forcing of contrail cirrus. *Nat Commun*. 2018;9(1):1824.

2. Schumann U. Formation, properties and climatic effects of contrails. *Comptes Rendus Phys*. 2005;6(4):549-565. doi:http://dx.doi.org/10.1016/j.crhy.2005.05.002

3. Schumann U. On conditions for contrail formation from aircraft exhausts. *Meteorol Zeitschrift*. 1996;5:4-23.

4. Jensen EJ, Toon OB, Kinne S, Sachse GW, Anderson BE, Chan KR, Twohy CH, Gandrud B, Heymsfield A, Miake-Lye RC. Environmental conditions required for contrail formation and persistence. *J Geophys Res Atmos*. 1998;103(D4):3929-3936.

5. Haywood JM, Allan RP, Bornemann J, Forster PM, Francis PN, Milton S, Rädel G, Rap A, Shine KP, Thorpe R. A case study of the radiative forcing of persistent contrails evolving into contrail-induced cirrus. *J Geophys Res Atmos*. 2009;114(D24201). doi:doi:10.1029/2009JD012650

6. Burkhardt U, Kärcher B. Process-based simulation of contrail cirrus in a global climate model. *J Geophys Res Atmos*. 2009;114(D16201). doi:doi:10.1029/2008JD011491

7. Ponater M, Marquart S, Sausen R. Contrails in a comprehensive global climate model: Parameterization and radiative forcing results. *J Geophys Res Atmos*. 2002;107(D13):ACL-2. doi:doi.org/10.1029/2001JD000429

8. Schumann U. A contrail cirrus prediction model. *Geosci Model Dev*. 2012;5:543-580.

9. Burkhardt U, Kärcher B. Global radiative forcing from contrail cirrus. *Nat Clim Chang*. 2011;1(1):54-58.

10. Mannstein H, Schumann U. Aircraft induced contrail cirrus over Europe. *Meteorol Zeitschrift*. 2005;14(4):549-554.

11. Meerkötter R, Schumann U, Doelling DR, Minnis P, Nakajima T, Tsushima Y. Radiative forcing by contrails. In: *Annales Geophysicae*. Vol 17. Springer; 1999:1080-1094.

12. Schumann U, Heymsfield AJ. On the lifecycle of individual contrails and contrail cirrus. *Meteorol Monogr*. 2017;58(1).

13. Schumann U, Graf K, Mannstein H, Mayer B. Contrails: Visible aviation induced climate impact. In: *Atmospheric Physics*. Springer; 2012:239-257.

14. Stuber N, Forster P, Rädel G, Shine K. The importance of the diurnal and annual cycle of air traffic for contrail radiative forcing. *Nature*. 2006;441(7095):864-867.

15. Lee DS, Pitari G, Grewe V, Gierens K, Penner JE, Petzold A, Prather MJ, Schumann U, Bais A, Berntsen T.

Transport impacts on atmosphere and climate: Aviation. *Atmos Environ*. 2010;44(37):4678-4734.

16. Schumann U, Graf K, Mannstein H. Potential to reduce the climate impact of aviation by flight level changes. In: *3rd AIAA Atmospheric Space Environments Conference*. Honolulu, Hawaii: American Institute of Aeronautics and Astronautics; 2011. doi:10.2514/6.2011-3376

17. Schumann U, Penner JE, Chen Y, Zhou C, Graf K. Dehydration effects from contrails in a coupled contrail–climate model. *Atmos Chem Phys*. 2015;15(19):11179-11199.

18. Myhre G, Kvalevåg M, Rädel G, Cook J, Shine KP, Clark H, Karcher F, Markowicz K, Kardas A, Wolkenberg P, Balkanski Y, Ponater M, Forster P, Rap A, Leon R, Rodriguez. Intercomparison of radiative forcing calculations of stratospheric water vapour and contrails. *Meteorol Zeitschrift*. 2009;18(6):585-596. doi:10.1127/0941-2948/2009/0411

19. Lim Y, Gardi A, Sabatini R. Optimal Aircraft Trajectories to Minimize the Radiative Impact of Contrails and CO 2. *Energy Procedia*. 2017;110:446-452.

20. Schumann U, Mayer B, Graf K, Mannstein H. A parametric radiative forcing model for contrail cirrus. *J Appl Meteorol Climatol*. 2012;51(7):1391-1406.

21. Lewellen DC, Lewellen WS. The Effects of Aircraft Wake Dynamics on Contrail Development. *J Atmos Sci*. 2001;58(4):390-406. doi:10.1175/1520-0469(2001)058<0390:TEOAWD>2.0.CO;2

22. Naiman AD, Lele SK, Wilkerson JT, Jacobson MZ. Parameterization of subgrid plume dilution for use in large-scale atmospheric simulations. *Atmos Chem Phys*. 2010;10(5):2551-2560. doi:10.5194/acp-10-2551-2010

23. Unterstrasser S, Sölch I. Study of contrail microphysics in the vortex phase with a Lagrangian particle tracking model. *Atmos Chem Phys*. 2010;10(20):10003-10015. doi:10.5194/acp-10-10003-2010

24. Lewellen DC. Persistent contrails and contrail cirrus. Part II: Full lifetime behavior. *J Atmos Sci*. 2014;71(12):4420-4438.

25. Caiazzo F, Agarwal A, Speth RL, Barrett SRH. Impact of biofuels on contrail warming. *Environ Res Lett*. 2017;12(11):114013.

26. Teoh R, Stettler MEJ, Majumdar A, Schumann U, Graves B, Boies A. A methodology to relate black carbon

particle number and mass emissions. *J Aerosol Sci*. 2019;132:44-59. doi:10.1016/J.JAEROSCI.2019.03.006

27. Agarwal A, Speth RL, Fritz TM, Jacob SD, Rindlisbacher T, Iovinelli R, Owen B, Miake-Lye RC, Sabnis JS, Barrett SRH. SCOPE11 Method for Estimating Aircraft Black Carbon Mass and Particle Number Emissions. *Environ Sci Technol*. 2019;53(3):1364-1373. doi:10.1021/acs.est.8b04060

28. Williams V, Noland RB. Variability of contrail formation conditions and the implications for policies to reduce the climate impacts of aviation. *Transp Res Part D Transp Environ*. 2005;10(4):269-280. doi:http://dx.doi.org/10.1016/j.trd.2005.04.003

29. Irvine EA, Hoskins BJ, Shine KP. A simple framework for assessing the trade-off between the climate impact of aviation carbon dioxide emissions and contrails for a single flight. *Environ Res Lett*. 2014;9(6):64021.

30. Mannstein H, Spichtinger P, Gierens K. A note on how to avoid contrail cirrus. *Transp Res Part D Transp Environ*. 2005;10(5):421-426. doi:http://dx.doi.org/10.1016/j.trd.2005.04.012

31. Grewe V, Matthes S, Frömming C, Brinkop S, Jöckel P, Gierens K, Champougny T, Fuglestvedt J, Haslerud A, Irvine E. Feasibility of climate-optimized air traffic routing for trans-Atlantic flights. *Environ Res Lett*. 2017;12(3):34003.

32. Moore RH, Thornhill KL, Weinzierl B, Sauer D, D'Ascoli E, Kim J, Lichtenstern M, Scheibe M, Beaton B, Beyersdorf AJ. Biofuel blending reduces particle emissions from aircraft engines at cruise conditions. *Nature*. 2017;543(7645):411-415.

33. Burkhardt U, Bock L, Bier A. Mitigating the contrail cirrus climate impact by reducing aircraft soot number emissions. *npj Clim Atmos Sci*. 2018;1(37):1-7. doi:doi:10.1038/s41612-018-0046-4

34. Boies AM, Stettler MEJ, Swanson JJ, Johnson TJ, Olfert JS, Johnson M, Eggersdorfer ML, Rindlisbacher T, Wang J, Thomson K. Particle emission characteristics of a gas turbine with a double annular combustor. *Aerosol Sci Technol*. 2015;49(9):842-855.

35. Lobo P, Durdina L, Smallwood GJ, Rindlisbacher T, Siegerist F, Black EA, Yu Z, Mensah AA, Hagen DE, Miake-Lye RC. Measurement of aircraft engine non-volatile PM emissions: Results of the aviation-particle regulatory instrumentation demonstration experiment (A-PRIDE) 4 campaign. *Aerosol Sci Technol*.

2015;49(7):472-484.

36. Eyers CJ, Addleton D, Atkinson K, Broomhead MJ, Christou R, Elliff T, Falk R, Gee I, Lee DS, Marizy C, Michot S, Middel J, Newton P, Norman P, Plohr M, Raper D, Stanciou N. AERO2K global aviation emissions inventories for 2002 and 2025. *QinetiQ Eur Comm under Contract No G4RD-CT-2000-00382, Farnborough, Hampshire, GU14 0LX, pp, 2005*. 2005.

37. Wilkerson JT, Jacobson MZ, Malwitz A, Balasubramanian S, Wayson R, Fleming G, Naiman AD, Lele SK. Analysis of emission data from global commercial aviation: 2004 and 2006. *Atmos Chem Phys*. 2010;10(13):6391-6408.

38. Simone NW, Stettler MEJ, Barrett SRH. Rapid estimation of global civil aviation emissions with uncertainty quantification. *Transp Res Part D Transp Environ*. 2013;25:33-41. doi:http://dx.doi.org/10.1016/j.trd.2013.07.001

39. Shigetomi S, Matsuda H, Kozuka T, Miyazawa Y. An Evaluation of CARATS Open Data Accuracy (Japanese Title: CARATS Open Data の精度に関する一検討). *Aerosp Technol Japan*. 2016;15:15-21.

40. Eurocontrol. *User Manual for the Base of Aircraft Data (BADA) Revision 3.12.* Vol EEC Techni. Eurocontrol Experimental Centre; 2014. https://www.eurocontrol.int/sites/default/files/field_tabs/content/documents/sesar/user-manual-bada-3-12.pdf.

41. Stettler MEJ, Eastham S, Barrett SRH. Air quality and public health impacts of UK airports. Part I: Emissions. *Atmos Environ*. 2011;45(31):5415-5424. doi:http://dx.doi.org/10.1016/j.atmosenv.2011.07.012

42. Wasiuk DK, Lowenberg MH, Shallcross DE. An aircraft performance model implementation for the estimation of global and regional commercial aviation fuel burn and emissions. *Transp Res Part D Transp Environ*. 2015;35:142-159.

43. Nuic A, Poles D, Mouillet V. BADA: An advanced aircraft performance model for present and future ATM systems. *Int J Adapt Control Signal Process*. 2010;24(10):850-866. doi:10.1002/acs.1176

44. Harada A, Miyamoto Y, Miyazawa Y, Funabiki K. Accuracy evaluation of an aircraft performance model with airliner flight data. *JSASS Aerosoace Tech Japan*. 2013.

https://www.jstage.jst.go.jp/article/tastj/11/0/11_TJSAS-D-13-00017/_article/-char/ja/. Accessed February 11, 2019.

45. Abrahamson JP, Zelina J, Andac MG, Vander Wal RL. Predictive Model Development for Aviation Black Carbon Mass Emissions from Alternative and Conventional Fuels at Ground and Cruise. *Environ Sci Technol*. 2016;50(21):12048-12055.

46. Anderson BE, Beyersdorf AJ, Hudgins CH, Plant J V, Thornhill KL, Winstead EL, Ziemba LD, Howard R, Corporan E, Miake-Lye RC. Alternative aviation fuel experiment (AAFEX). *Rep No NASA/TM-2011-217059*. 2011.

47. Stettler MEJ, Boies A, Petzold A, Barrett SRH. Global civil aviation black carbon emissions. *Environ Sci Technol*. 2013;47(18):10397-10404.

48. Wey CC, Anderson BE, Hudgins C, Wey C, Li-Jones X, Winstead E, Thornhill LK, Lobo P, Hagen D, Whitefield P. Aircraft particle emissions experiment (APEX). 2006.

49. EASA. ICAO Aircraft Engine Emissions Databank. https://www.easa.europa.eu/document-library/icao-aircraft-engine-emissions-databank. Published 2011.

50. ECMWF. Forecast User Guide - 5.1 Generation of the Ensemble, Ensemble of Data Assimilations (EDA). https://confluence.ecmwf.int/display/FUG/Ensemble+of+Data+Assimilations+-+EDA. Published 2019.

51. Schumann U, Mayer B. Sensitivity of surface temperature to radiative forcing by contrail cirrus in a radiative-mixing model. *Atmos Chem Phys, 17, 13833–13848*. 2017. doi: 10.5194/acp-17-13833-2017.

52. Hansen J, Sato M, Ruedy R, Nazarenko L, Lacis A, Schmidt GA, Russell G, Aleinov I, Bauer M, Bauer S, Bell N, Cairns B, Canuto V, Chandler M, Cheng Y, Genio A Del, Faluvegi G, Fleming E, Friend A, et al. Efficacy of climate forcings. *J Geophys Res*. 2005;110(D18):D18104. doi:10.1029/2005JD005776

53. Ponater M, Marquart S, Sausen R, Schumann U. On contrail climate sensitivity. *Geophys Res Lett*. 2005;32(10).

54. Rap A, Forster PM, Haywood JM, Jones A, Boucher O. Estimating the climate impact of linear contrails using the UK Met Office climate model. *Geophys Res Lett*. 2010;37(20). doi:10.1029/2010GL045161

55. NASA. By the Numbers | Earth – NASA Solar System Exploration.

https://solarsystem.nasa.gov/planets/earth/by-the-numbers/. Accessed November 27, 2019.

56. Joos F, Roth R, Fuglestvedt JS, Peters GP, Enting IG, von Bloh W, Brovkin V, Burke EJ, Eby M, Edwards NR, Friedrich T, Frölicher TL, Halloran PR, Holden PB, Jones C, Kleinen T, Mackenzie FT, Matsumoto K, Meinshausen M, et al. Carbon dioxide and climate impulse response functions for the computation of greenhouse gas metrics: a multi-model analysis. *Atmos Chem Phys*. 2013;13(5):2793-2825. doi:10.5194/acp-13-2793-2013

57. Schumann U, Schlager H, Arnold F, Ovarlez J, Kelder H, Hov Ø, Hayman G, Isaksen ISA, Staehelin J, Whitefield PD. Pollution from aircraft emissions in the North Atlantic flight corridor: Overview on the POLINAT projects. *J Geophys Res Atmos*. 2000;105(D3):3605-3631. doi:10.1029/1999JD900941

58. Schumann U, Arnold F, Busen R, Curtius J, Kärcher B, Kiendler A, Petzold A, Schlager H, Schröder F, Wohlfrom K. Influence of fuel sulfur on the composition of aircraft exhaust plumes: The experiments SULFUR 1–7. *J Geophys Res Atmos*. 2002;107(D15).

59. Jeßberger P, Voigt C, Schumann U, Sölch I, Schlager H, Kaufmann S, Petzold A, Schäuble D, Gayet J-F. Aircraft type influence on contrail properties. *Atmos Chem Phys*. 2013;13(23):11965-11984.

60. Schumann U, Baumann R, Baumgardner D, Bedka S, Duda D, Freudenthaler V, Gayet J-F, Heymsfield AJ, Minnis P, Quante M. Properties of individual contrails: A compilation of observations and some comparisons. *Atmos Chem Phys Discuss*. 2017:1-62.

61. Schumann U, Graf K. Aviation-induced cirrus and radiation changes at diurnal timescales. *J Geophys Res Atmos*. 2013;118(5):2404-2421.

62. Schumann U, Jeßberger P, Voigt C. Contrail ice particles in aircraft wakes and their climatic importance. *Geophys Res Lett*. 2013;40(11):2867-2872.

63. Vázquez-Navarro M, Mannstein H, Kox S. Contrail life cycle and properties from 1 year of MSG/SEVIRI rapid-scan images. *Atmos Chem Phys*. 2015;15(15):8739-8749. doi:10.5194/acp-15-8739-2015

64. Spichtinger P, Gierens K, Leiterer U, Dier H. Ice supersaturation in the tropopause region over Lindenberg, Germany. *Meteorol Zeitschrift*. 2003;12(3):143-156.

65. Filippone A. Assessment of aircraft contrail avoidance strategies. *J Aircr*. 2015;52(3):872-877.

66. Kärcher B. The importance of contrail ice formation for mitigating the climate impact of aviation. *J Geophys Res Atmos*. 2016;121(7):3497-3505.

67. Bock L, Burkhardt U. Contrail cirrus radiative forcing for future air traffic. *Atmos Chem Phys*. 2019;19(12):8163-8174. doi:10.5194/acp-19-8163-2019

68. Stuber N, Ponater M, Sausen R. Why radiative forcing might fail as a predictor of climate change. *Clim Dyn*. 2005;24(5):497-510. doi:10.1007/s00382-004-0497-7